Scientific Reports

https://doi.org/10.1038/s41598-026-40330-y

Article in Press

Millimeter-wave technology for multi-person fall detection validated through wearable sensors and real-life scenarios

Received: 13 October 2025

Accepted: 12 February 2026

Published online: 25 February 2026

Cite this article as: Chen H., Lin J., Lin S. *et al.* Millimeter-wave technology for multi-person fall detection validated through wearable sensors and real-life scenarios. *Sci Rep* (2026). https://doi.org/10.1038/s41598-026-40330-y

Hsiang-Ho Chen, Jui-Da Lin, Shu-Hsuan Lin, Chieh-Wei Wu & Hsin-Chang Chen

Millimeter-wave Technology for Multi-person Fall Detection Validated Through Wearable Sensors and Real-life Scenarios

Hsiang-Ho Chen[1,2,+], Jui-Da Lin[1,+], Shu-Hsuan Lin[1], Chieh-Wei Wu[1], and Hsin-Chang Chen[1,3,4,5,*]

[1]Chang Gung University, Department of Biomedical Engineering, Taoyuan City, 333, Taiwan(R.O.C.)
[2]Linkou Chang-Gung Memorial Hospital, Department of Plastic and Reconstructive Surgery, Taoyuan City, 333, Taiwan(R.O.C.)
[3]Taipei City Hospital, Department of Orthopedic Surgery Heping Branch, Taipei City, Taiwan(R.O.C.)
[4]National Yang Ming Chiao Tung University, Faculty of Medicine School of Medicine, Taipei City, Taiwan(R.O.C.)
[5]University of Taipei, Department of Exercise and Health Sciences, Taipei city, Taiwan(R.O.C.)
[*]Corresponding author: Hsin-Chang Chen. Email: dau26@tpech.gov.tw
[+]these authors contributed equally to this work

ABSTRACT

Background: Older adults face increased health risks, especially accidental injuries such as falls, which are one of the top ten causes of death in this age group. To address these changes, recent innovations have focused on developing advanced monitoring technologies to detect and prevent accidents in real time. Among these, fall detection systems have emerged as a critical area of research. This study aimed to evaluate the ability of millimeter-wave (mmWave) sensors to accurately detect multiple falls in the presence of large obstacles in a large, real-world indoor space. **Methods:** The mmWave sensors employed the Doppler effect to capture a human body's point cloud and track its center point to estimate body position and identify fall events. A 12 × 12 meter indoor test area was established for the trials. The mmWave system's accuracy was validated with video ground truth. Multiple sensors and azimuth tests were conducted to optimize radar configurations. 10 participants performed multiple human fall detection trials under 10 different scenarios. **Results:** We have successfully validated the mmWave system with the video ground truth. In fall detection testing, the mmWave system achieved an overall accuracy of 97.9% across 10 multi-person scenarios. The results show that the system's fall detection false negative rate increases with the number of subjects. **Conclusion:** This study validated the performance of a mmWave system for fall detection in a large indoor environment, demonstrating a high accuracy of 97.9% in a multi-person scenario. However, performance varied with crowd density, showing a correlation between increased false negative rates and the number of subjects due to occlusion. This study supports that mmWave technology offers good capabilities for fall accident monitoring in large indoor spaces with both privacy protection and convenience.
IRB Registry: Institutional Review Board of the Chang Gung Medical Foundation, Approval No.: 202500191B0, Registration date: 3 March 2025.

Keywords: mmWave, Fall detection, Posture, Older adults, IMU

Introduction

The World Health Organization (WHO) predicts that the percentage of people over 60 will nearly double from 12% to 22% between 2015 and 2050. This trend reflects the global aging situation. As society ages, we need supportive environments and medical services to address this change. Cardiovascular disease is the leading cause of death among older adults, followed by cancer. Unintentional injuries, like falls, are also among the top ten causes of death[1]. Therefore, older adults require more specialized care and monitoring throughout the day, which is provided in long-term care (LTC). LTC includes help with daily activities such as bathing, dressing, eating, and moving, as well as support for managing chronic illnesses and medications. The aim is to improve the quality of life for elderly individuals while ensuring their safety and well-being. Whether in care centers or through home services, long-term care for the elderly relies heavily on human monitoring throughout the day. However, this approach can still have gaps, and accidents often occur in an instant. To prevent and reduce these incidents, the market has recently seen the development of more advanced monitoring devices. A 2023 market research report highlights that safety and risk management systems for the elderly are emerging as key trends in the future development of healthcare, underscoring the need for innovation in this critical area[2]. For over a decade, many activity detection devices have

been developed. Feng et al. demonstrated fall detection in a bathroom using a pressure sensor to identify target postures and determine fall events based on changes in body weight on the ground[3]. However, this system struggles to distinguish the human body from other objects in the same space. In contrast, Lin et al. presented real-time monitoring with a chest-worn inertial measurement units (IMU) to detect falls and recognize activities[4,5]. However, the effectiveness of wearable devices relies heavily on user compliance. Frequent false alarms can significantly reduce this compliance, discouraging older adults from wearing these devices[6]. Additionally, camera-based monitoring systems are restricted from private spaces, affecting their coverage and accuracy. In contrast, mmWave technology offers a potential solution, providing non-contact monitoring, privacy protection, convenience, and remote monitoring capabilities. mmWave-based monitoring systems leverage the Doppler effect[7,8] and have been extensively studied for various applications, including fall detection[9], human activity recognition[10], vital sign monitoring[11,12], and human posture identification[13]. Previous studies of mmWave fall detection focus on a small detection area with a few human subjects (a maximum of 3 people)[9,10,14,15]. Different data retrieved from mmWave were used to detect fall events, including three-dimensional (3D) Point cloud[9,10,14,15], Range-Time, Doppler Time Map[16], Range-velocity, Range-angle Map[17], one-dimensional (1D) point cloud, and Doppler velocity[18]. Although they demonstrate high accuracy in all literature (ranging from 92.2%-99.5%), large real-life indoor scenarios have never been discussed, which makes these studies less relevant to real-life scenarios. This study aims to evaluate the performance of mmWave fall detection technology in large, real-world indoor areas, including structural columns, by simulating various fall scenarios. In addition to video recording to confirm the occurrence of falls, a chest-mounted IMU sensor was used to assist in detecting the timing of falls. Positioning error analysis was then used to evaluate the performance of the mmWave system in detecting human falls. This research can provide a reference for establishing fall detection and monitoring systems using mmWave technology in public places, such as long-term care facilities for the elderly and hospitals, hoping to provide faster assistance and reduce social healthcare costs.

Methods

Study Design

This study evaluates the performance of mmWave radar technology for fall detection in a large-scale, real-world indoor environment. The experimental framework was conducted in a 12×12 m area with the following five main objectives:

1. Establishing a fall detection zone within a 12×12 m real-life indoor scenario
2. Validating the mmWave radar data with video ground truth
3. Assessing the mmWave system's detection accuracy across multi-radar mmWave configurations
4. Evaluating the mmWave system's capability to detect falls in multiple human fall detection
5. Testing the mmWave system's robustness by fall-Like activities of daily living detection trials

To rigorously test these objectives, 10 healthy adult participants (6 males and 4 females) were recruited to perform a series of trials under the aforementioned configurations.

Ethical Approval and Informed Consent

All study procedures were conducted in accordance with the ethical standards of the Chang Gung Medical Foundation Institutional Review Board (IRB) and with relevant national and international guidelines and regulations. The research protocol was reviewed and approved by the Institutional Review Board of the Chang Gung Medical Foundation, approval number 202500191B0. Informed consent was obtained from all subjects before participation; all participants were over 18 years of age.

Principles of mmWave Monitoring

mmWave monitoring technology is based on Frequency Modulated Continuous Wave (FMCW) radar, utilizing the Doppler principle to detect distance and motion. FMCW radar transmits a continuously modulated mmWave signal over time, referred to as the transmitter radio frequency (Tx (1)), while receiving the reflected mmWave signal, known as the receiver radio frequency (Rx (2)). Each continuously transmitted mmWave signal is termed a chirp. By calculating the time delay between Tx and Rx, the distance of the target object could be estimated. However, to further monitor the movement of the object, the Tx and Rx signals must be mixed using a mixer, generating an intermediate frequency signal (IF). Setting intermediate frequency signal phase data as a reference, the phase variations between Tx and Rx can be computed to obtain the phase difference, which is further calculated into the object's velocity[19,20]. The amplitude of the transmitted frequency (Tx) is presented as equation (1):

$$\gamma_T(t) = A_T \times \sin\left(2\pi \times (f_0 + K \times t) \times t\right) \quad (1)$$

A_T: signal transmission amplitude, K: frequency modulation slope, f_0: Initial frequency of the transmitted wave.

The amplitude of the received frequency (Rx) is presented as equation (2):

$$\gamma_R(t) = A_R \times \sin\left(2\pi \times (f_0 + K \times (t-\delta)) \times (t-\delta)\right) \tag{2}$$

d: target distance, υ: speed of the electromagnetic wave, $\delta = \frac{2\times d}{\upsilon}$

Monitoring real-time two-dimensional (2D) or three-dimensional (3D) dynamics of multiple objects or surfaces (e.g., the human body) requires the FMCW radar to employ a multiple-input multiple-output (MIMO) radar system[21]. This system incorporates multiple transmission and reception channels. Raw data is analyzed and processed through algorithms to determine and recognize human activity states, a widely adopted approach in contemporary research[22]. Other studies infer 3D monitoring parameters by analyzing multiple transmitted and received wave signals. In 3D space, the radar system manipulates the multiple detection points system on the human body surface, forming a point cloud. The mmWave system can effectively identify, locate, and interpret the activity states of a human through tracking the center of mass (COM) of the point cloud.

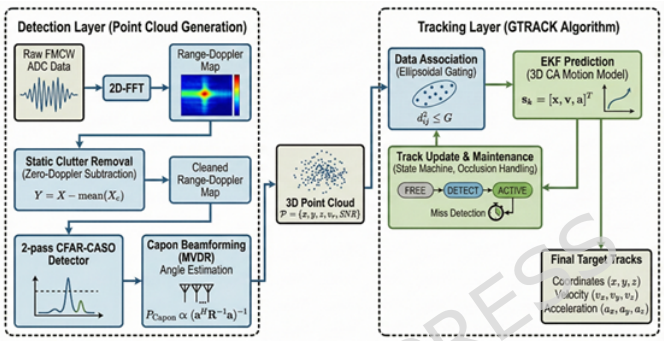

Figure 1. Data Processing flow chart of the mmWave System

Data Processing and Tracking Algorithm of the mmWave System

The signal processing pipeline, illustrated in Figure 1, consists of two primary stages: (1) the Detection Layer, which converts raw analog-to-digital-converter (ADC) data into a 3D point cloud, and (2) the Tracking Layer, which aggregates points into target tracks of COM using a Group Tracking algorithm.

Detection Layer: Point Cloud Generation

The raw FMCW ADC data is processed via a 2D Fractional Fourier Transform (2D-FFT) to generate a Range-Doppler Map. To mitigate stationary interference (e.g., walls, furniture), a Static Clutter Removal algorithm is applied by subtracting the mean of the complex samples across chirps in the zero-Doppler bin:

$$Y(r,d) = X(r,d) - \frac{1}{N_c}\sum_{c=0}^{N_c-1} X(r,d)_c \tag{3}$$

where $Y(r,d)$ is the clutter-removed signal, $X(r,d)$ represents the original Range-Doppler spectrum at range bin r and Doppler bin d, and N_c denotes the number of chirps per frame used for averaging the static component. Subsequently, significant scattering points are detected using a 2-pass CFAR-CASO (Cell-Averaging Smallest of Constant False Alarm Rate) algorithm. This method is robust against non-homogeneous clutter edges common in indoor environments. For angle estimation, we employ the Capon Beamforming (MVDR) technique. The Capon estimator computes the spatial power spectrum $P_{Capon}(\theta,\phi)$ by minimizing the variance of the output while maintaining unity gain in the look direction:

$$P_{Capon}(\theta,\phi) = \frac{1}{a^H(\theta,\phi)\widehat{R}_{xx}^{-1}a(\theta,\phi)} \tag{4}$$

where θ and ϕ represent the azimuth and elevation angles respectively, $a(\theta,\phi)$ is the steering vector corresponding to the antenna array geometry, $(\cdot)^H$ denotes the Hermitian transpose, and $\widehat{R}_{xx}$ is the estimated spatial covariance matrix of the received signal. This results in a sparse 3D point cloud $P_{local} = \{x, y, z, v_r, SNR\}$ serving as input to the tracker.

Tracking Layer: Group Tracker (GTRACK)

To track multiple subjects and handle occlusion, the standard Group Tracker (GTRACK) algorithm was implemented, which was also mentioned in previous studies[14, 18, 23].

1.Extended Kalman Filter:

The tracker utilizes an Extended Kalman Filter (EKF) with a 3D Constant Acceleration (CA) motion model to handle non-linear spherical-to-Cartesian transformations. The state vector $\mathbf{s}_k$ at time step k is defined as:

$$\mathbf{s}_k = [x, y, z, v_x, v_y, v_z, a_x, a_y, a_z]^T \tag{5}$$

where x, y, z denote the 3D position, v_x, v_y, v_z denote the velocity components, and a_x, a_y, a_z denotes the acceleration components. The state prediction follows the physical model:

$$\hat{\mathbf{s}}_{k|k-1} = \mathbf{F}\mathbf{s}_{k-1|k-1} + Q_k \tag{6}$$

where $\hat{\mathbf{s}}_{k|k-1}$ is the predicted state vector, $\mathbf{F}$ is the state transition matrix for the constant acceleration model, $\mathbf{s}_{k-1|k-1}$ is the updated state from the previous step, and Q_k represents the process noise covariance matrix accounting for model uncertainties.

2.Ellipsoidal Gating:

Association of new measurement points to existing tracks is performed using Ellipsoidal Gating. We compute the Mahalanobis Distance d^2 between a measurement point u_j and the predicted track centroid, normalized by the Group Residual Covariance Matrix C_G:

$$d_{ij}^2 = \left(u_j - H(\hat{\mathbf{s}}_{k|k-1})\right)^T C_G^{-1} \left(u_j - H(\hat{\mathbf{s}}_{k|k-1})\right) \leq G \tag{7}$$

where u_j is the measurement vector (range, azimuth, elevation, Doppler) of the j-th point, $H(\cdot)$ is the non-linear measurement function converting the predicted state to spherical coordinates, and G is the gating gain parameter. The matrix C_G accounts for the target's estimated physical size (dispersion), maneuvering error, and measurement noise.

3. Track Maintenance and Occlusion Handling:

The tracker employs a probabilistic State Machine (FREE $\rightarrow$ DETECT $\rightarrow$ ACTIVE). To address the reviewer's concern regarding occlusion (e.g., a subject moving behind the structural column), the system utilizes a "Miss Detection" logic. When a target is occluded, the Association step fails to find matching points. However, the track remains in the ACTIVE state for a configurable duration (defined by the active2freeThre parameter, typically set to 1-2 seconds). During this period, the EKF continues to propagate the target's position based on its last known velocity and acceleration, ensuring ID stability until the subject re-emerges.

Multi-Radar Data Fusion:

To achieve cross-radar data fusion covering the 12x12m area, the target tracks generated by each radar's GTRACK instance are transformed into a unified World Coordinate System (WCS). In overlapping or adjacent detection zones, different radars may simultaneously track the same or proximal targets. To prevent duplicate counting and enhance localization precision, the system compares and merges tracks that are spatially close in the world frame.

1. Coordinate Transformation Let $P_{local}^i = [x_s, y_s, z_s]^T$ be the detected target position from the i-th radar. The global coordinate P_{world} is computed via a rigid body transformation:

$$P_{world} = R_i \cdot P_{local}^i + t_i \tag{8}$$

where $R_i \in \mathbb{R}^{3\times3}$ is the rotation matrix derived from the sensor's mounting angles (azimuth α, elevation β), and $t_i = [t_x, t_y, t_z]^T$ is the translation vector representing the sensor's physical position.

2. Nearest Neighbor Association & Merging

The merging process employs a Nearest Neighbor Search algorithm to determine the correlation between targets from different sensors. We calculate the Euclidean distance d_{mn} between track m from Sensor A and track n from Sensor B is calculated as:

$$d_{mn} = \|P_{world}^m - P_{world}^n\|_2 \tag{9}$$

If d_{mn} falls below the threshold λ_{merge} (set at 0.5m), the system treats them as the same entity. The final fused position P_{fused} is computed as the average of the matched target coordinates:

$$P_{fused} = \frac{1}{N_{sensors}} \sum_{k=1}^{N_{sensors}} P_{world}^k \tag{10}$$

This fusion approach not only improves coordinate accuracy but also effectively unifies detection results across multiple radars. Furthermore, simultaneous observation from multiple radars at different angles ensures that a target, even if occluded in the field of view of specific sensors (e.g., by the structural column), can still be identified via supplementary information from other radars. This fused data mitigates occlusion risks caused by viewing angles, thereby enhancing overall detection stability and reliability.

Feature Extraction

The raw data collected includes the vertical height (P_z) of the subjects' COM and the timestamp. To capture the dynamic characteristics of fall events, kinematic features were derived as follows for each time frame t:

1. **Vertical Velocity (V_z):** Calculated as the first derivative of height with respect to time. Negative values indicate downward movement.

2. **Vertical Acceleration (A_z):** Calculated as the second derivative of height.

3. **Frame-to-Frame Difference ($D_{neighbor}$):** The absolute difference in height between the current frame and its neighbors ($|P_z(t) - P_z(t-1)|$ and $|P_z(t) - P_z(t+1)|$), used to detect sudden discontinuities.

Fall Detection Algorithm

A two-phase detection algorithm was designed to balance sensitivity and false alarm rate. The algorithm distinguishes falls from non-fall activities.

- **Phase 1: Impact Trigger (Event Detection)** The system scans for high-velocity downward movements accompanied by a low posture. An "Impact Candidate" is flagged if any single frame satisfies:

  $$V_z(t) < \lambda_V \quad \text{AND} \quad P_z(t) < \lambda_P$$

  Where λ_V is the velocity threshold (negative value), and λ_P is the height threshold.

- **Phase 2: Post-Fall Confirmation (Stillness Check)** To filter out ADLs where the subject stands up immediately (e.g., tying shoes), we evaluate the final posture after a stabilization period (or at the end of the event window). A fall is confirmed only if:

  $$P_z(t_{end}) < \lambda_{still}$$

  Where λ_{still} is the stillness height threshold, and t_{end} denotes the timestamp at the end of the evaluation window.

To determine the optimal thresholds, Grid Search was performed over the parameter space defined below. Note that in addition to the primary triggers, we also optimized thresholds for acceleration (λ_A) and frame difference (λ_D) to refine detection boundaries:

- $\lambda_V \in [-0.4, -0.5, \ldots, -0.8]$ m/s
- $\lambda_D \in [0, 0.05, 0.1]$ m
- $\lambda_P \in [0.6, 0.7, \ldots, 1.0]$ m
- $\lambda_{still} \in [0.8, 0.9, 1.0, 1.2]$ m
- $\lambda_A \in [0, 1, 2, 5]$ m/s^2

The thresholds for the fall detection in the multi-person scenario trial were λ_P = 0.8 m, and λ_D = 0.1 m. In the additional fall-like ADLs trial, the thresholds were refined to λ_V = -0.60 m/s, λ_P = 1.0 m, λ_{still} = 1.0 m by the Grid Search, and with two parameters(λ_A, λ_D) disabled.

To further validate the thresholds (λ_V, λ_P, λ_{still}) and assess the model's generalization capability, we employed Leave-One-Out Cross-Validation (LOOCV) by iterating through the N=150 data files. In each iteration, one file was held out as the test set, while the remaining N-1 files served as the training set to optimize thresholds. Separately, for the final system deployment, the optimal parameters were derived using the full dataset. Where the thresholds were further refined to λ_V = -0.30 m/s, λ_P = 1.0 m, λ_{still} = 0.9 m.

mmWave radar system setting for 12 × 12 meters indoor area

The mmWave radar (MT5B9SE01K, Jorgen Technology Co., Ltd., Taiwan) was tested for its capability for detection precision in various azimuths before establishing the detection area. This radar is based on a single-chip mmWave radar (IWR6843, Texas Instruments, U.S.), features a short-range antenna with a broad field of view (FoV), and was used to detect real-time 3D point clouds in previous studies[9]. The pre-test result has shown that high accuracy of fall events at the detection azimuth angles of 45° to -45° (Receiver operating characteristic curve (ROC) = 0.937, $p < 0.001$), and optimal detection distance of 3-6 meters. According to the results of the pre-test, we designed the mmWave radar system setting with 4 radars placed at the corners to cover the large detection zone of 12 x 12 meters. To more closely simulate the real environment, we selected the testing scenario with a structural column in the center, which presented a more challenging environment than previous mmWave studies conducted in an open testing scenario[15]. A detection area measuring 12 × 12 meters was established, with 4 radar sensors positioned at the corners, all oriented towards the center of the area, and the detection zones were set at (1,1), (1,13), (13,1), and (13,13) (figure 2). The elevation angle of the radars was set at 15°, and the height was 2 meters, as determined by our pre-tests and previous studies[9,14,15]. The azimuth and elevation angles were carefully calibrated, and the radars were placed in proper distance to ensure that the detection zone was covered in the mmWave beam from floor to ceiling. All four radars were connected to the PC through USB cables and an extension with a signal amplifier, and were calibrated before each trial.

Validation of mmWave radar with video ground truth

The performance of the mmWave radar was evaluated using cross-validation with video ground truth. The time stamp of the IMU was extracted to validate the time delay of the mmWave system. The subjects were simultaneously monitored by the camera, mmWave, and chest-worn IMU sensor (Figure 2) while they underwent the fall trial within the mmWave detection area. Simulated scenarios were recorded by a camera and serve as video ground truth for validating the fall detection accuracy of the mmWave system. The criteria fall occurrence of the IMU measurement was defined as recommended in a past study (G value difference >600, as presented in equation (11))[4].

$$G\ value = \sqrt{Ax^2 + Ay^2 + Az^2} \tag{11}$$

The subjects were asked to freely walk in the detection area for at least 3 seconds and simulate the soft fall events. The procedure was repeated at least 90 times. The fall detection results were recorded 3 seconds after the subject simulated the fall events. 3 subjects participated in this trial, with a total of 270 simulated trial data recorded. Data from the human trial were recorded and sorted with Excel by the research team. Both systems' monitoring was synchronized through the time stamp in the data. IMU data was aligned with mmWave output using User Datagram Protocol (UDP) through timestamps collected from both systems during data processing.

Figure 2. Subject with a chest-worn IMU

Figure 3. Multiple human fall event trial of mmWave radar systems, red line indicates detection area

Multi-Radar mmWave Configurations

A total of 5 multiple configurations were tested to compare the differences in accuracy of coordinate and fall detection based on the number of sensors (Figure 4). The radars were calibrated and tested using the methods previously described. Each configuration was tested with 25 target locations scattered evenly within the detection zones. During the trial, the 1 subject was

asked to walk to stand on the pre-marked location and stand still for at least 3 seconds before recording the detected coordinates in the mmWave system. The subject was asked to simulate a fall right after researchers recorded the detected coordinates and maintain the position for at least 3 seconds before the detection record was taken. The trials were repeated 3 times for all 25 target locations.

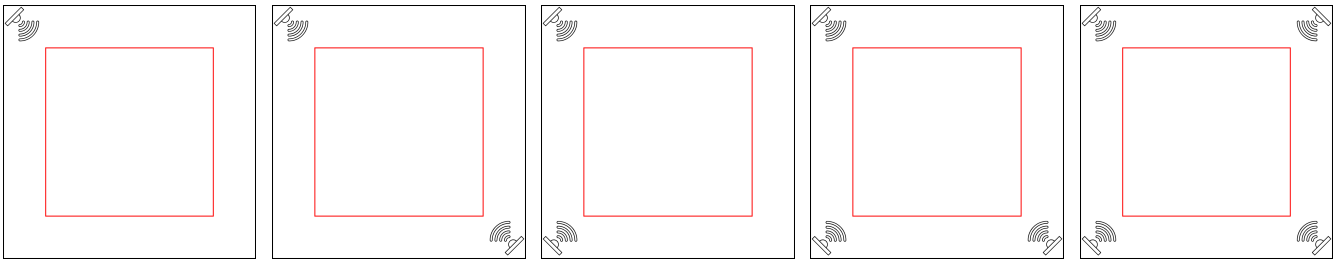

Figure 4. Multiple radar settings and the detection zone (red line): (a) Single set; (b) Diagonal 2 sets; (c) Same-side 2 sets; (d) 3 sets; (e) 4 sets of mmWave radars

Multiple Human Fall Detection

Multiple human fall trials were conducted within a 12x12 indoor area, including multiple subjects (up to 10) with various fall events to validate the system's accuracy Figure 3. The configuration of 4 radars was chosen according to the results of the multiple radar configuration test. A total of 10 test scenarios were conducted (with 1 to 10 subjects). Each round of the scenario starts with a countdown of three seconds; the subjects could randomly choose to simulate falling or standing still once the countdown ended. Detection results and the real status for each subject were recorded 3 seconds after the countdown ended. The procedure was repeated for at least 3 rounds until sufficient data were available for statistical analysis. The number of subjects who fell for each scenario was also recorded for further investigation.

Fall-Like Activities of Daily Living Detection

To further assess the mmWave system's detection capability between the fall-like Activities of Daily Living (ADLs), additional trials were conducted. With the identical experiment setup of a 12x12 indoor area, 10 subjects were recruited to perform 5 fall-like ADLs, including: rapid sitting, deep squatting, picking up a pen from the floor, tying shoes, and soft fall. Each subject was asked to perform 5 procedures for at least 3 rounds until sufficient data were available for statistical analysis.

Statistical analysis

The data of this study were analyzed through the correlation coefficient, confusion matrix, and ROC curve to evaluate the predictability of the mmWave system[9,15]. The cross-correlation analysis was used to investigate the time delay between IMU sensing and the mmWave system. All statistical analyses were performed using Python 3.11.0 statistical packages Pandas, NumPy, and SciPy[24].

Single-chip millimeter-wave radar

This project employs a single-chip intelligent mmWave sensor operating within the 60 GHz to 64 GHz frequency range, featuring integrated processing capabilities. The mmWave radar is characterized by its short wavelength, high resolution, multiple-input multiple-output (MIMO), and Antennas-On-Package (AOP) design, facilitating the development of a high-precision human limb recognition system. The chip processes and transmits data in JavaScript Object Notation (JSON) format via the User Datagram Protocol (UDP), ensuring rapid responsiveness in analyzing real-time scenarios involving the test subjects (Table 1).

Table 1. Technical Specifications of MT5B9SE01K

Parameter	Description
Frequency Modulation Range	60–64 GHz
Number of Receivers and Transmitters	4, 3 (Built-in)
Processor	Microcontroller Unit, Fast Fourier Transform accelerator, Digital Signal Processor
Memory	1.75 MB
Horizontal Field of View (FOV)	±60°
Horizontal Angular Resolution	29°
Vertical Field of View (FOV)	±60°
Vertical Angular Resolution	29°
Gain	5 dBi

Table 2. Technical Specifications of IMU (Movella DOT)

Parameter	Description
Wearing Method	Strap-based
Sensors	17 independent wireless sensors
Battery Life	9.5 hours per charge
Wireless Transmission Range	200 meters
Output Frequency	60 Hz

Movella DOT inertial measurement unit

The motion data recorded by an IMU was used as a time stamp reference to the mmWave system. The IMU (Movella DOT, Movella Inc., Henderson, NV, U.S.) is capable of capturing the velocity, acceleration, orientation, angular velocity, and angular acceleration of the human body in real time. It allows for immediate recording, previewing, and playback of motion capture data. Data was collected at a sampling rate of 60 Hz for various motion parameters, including position, velocity, acceleration, orientation, angular velocity, and angular acceleration (Table 2).

Results

Accuracy of a single radar at different azimuth angles and distances

The azimuth angle of the mmWave radar showed a correlation with the error distance of the estimated x-y coordinates (r_s = 0.191, p = 0.004). Notably, 60° and -60° azimuth angles produced weak detection signals, yielding only 3% and 33% of the effective detection data, Table 3. Monitoring distance was also correlated to error distance (r_s = 0.243, p < 0.001). The radar chart was drawn using the error distance of every data cell to further visualize the best detection zone of a mmWave radar sensor.

Table 3. Error distance of a single mmWave radar

Distance (m)	Azimuth angles								
	-60	-45	-30	-15	0	15	30	45	60
0.5	N/A	0.386248	N/A	N/A	N/A	N/A	N/A	N/A	N/A
1	0.124	0.147	0.091	0.039	0.071	0.049	0.059	0.134	N/A
1.5	0.125	0.121	0.127	0.108	0.045	0.037	0.169	0.179	N/A
2	0.177	0.071	0.101	0.044	0.092	0.094	0.129	0.201	0.175
2.5	0.119	0.135	0.181	0.213	0.224	0.091	0.064	0.048	N/A
3	N/A	0.122	0.150	0.188	0.197	0.080	0.080	0.062	N/A
3.5	N/A	0.057	0.147	0.118	0.108	0.091	0.171	0.136	N/A
4	0.181	0.202	0.182	0.114	0.074	0.033	0.212	N/A	N/A
4.5	0.188	0.164	0.153	0.153	0.092	0.079	0.199	N/A	N/A
5	0.170	0.206	0.192	0.120	0.094	0.085	0.276	N/A	N/A
5.5	N/A	0.063	0.066	0.128	0.164	0.148	0.264	0.376	N/A
6	N/A	0.078	0.119	0.116	0.215	0.101	0.643	0.438	N/A

Accuracy of 5 different radar configurations

Different radar configurations showed the best fall detection rate of 95% at 4-device sets of radars (ROC = 0.947, p < 0.001), followed by 3-device (ROC = 0.900, p < 0.001), 2-device Diagonal (ROC = 0.887, p < 0.001),1-device (ROC = 0.847, p < 0.001), 2-device same-side (ROC = 0.800, p < 0.001) (Table 4). On the other hand, the error distance was negatively correlated with the device quantity of radar sets (r_s = -0.283, p < 0.001). In these 5 different sets of radar, the 2-device Diagonal set has the best performance on the error distance (Median, interquartile range) (0.084 m, 0.121-0.194), followed by 4-device (0.091 m, 0.06-0.130), 3-device (0.108 m, 0.066-0.143), 2-device same-side (0.112 m, 0.080-0.143), 1-device (0.161 m, 0.121-0.194). The 2-device Diagonal set showed a significant difference to the 2-device same-side (0.084 m, 0.121-0.194) vs. 0.112 m,

0.080-0.143, $p < 0.001$) and 1-device sets (0.084 m, 0.121-0.194 vs. 0.161 m, 0.121-0.194, $p = 0.027$) respectively Table 4. The results indicate that multiple device radar sets could slightly improve the detection accuracy, and setting the device diagonally performed better than setting the device on the same side.

Table 4. Statistical analysis of different radar configurations

	ROC	p value	Error distance (m)
4-device	0.947	< 0.001	0.091 (0.060–0.130)
3-device	0.900	< 0.001	0.108 (0.066–0.143)
2-device Diagonal	0.887	< 0.001	† § 0.084 (0.121–0.194)
2-device same-side	0.800	< 0.001	† 0.112 (0.080–0.143)
1-device	0.847	< 0.001	§ 0.161 (0.121–0.194)

†: significant difference between 2-device Diagonal vs. 2-device same-side, p<0.001
§: significant difference between 2-device Diagonal vs. 1-device, p=0.027

Accuracy of the radar system in multi-person scenarios

In fall detection testing, the mmWave system achieved an overall high accuracy of 97.9% across all scenarios (1-10 subjects) despite the presence of the structural column in a 12 × 12 meter indoor environment (Figure 5). The highest accuracy was achieved with 1 and 4 subject scenarios (both ROC = 0.994, $p < 0.001$), while the lowest accuracy was achieved with 10 people (ROC = 0.967, $p < 0.001$), Table 5. Further statistical analysis between scenarios shows a trend of the system's type II error (False Negative rate, FNR) increases with the number of subjects (Figure 6). The highest FNR was observed at the scenario of 10 people (0.065), and the lowest was observed in the trials of 1 and 4 people scenarios. Further correlation analysis demonstrates a strong positive correlation between the number of people and FNR ($r = 0.895$, $p < 0.001$). This is likely due to the signal interruptions when the system simultaneously tracks multiple subjects.

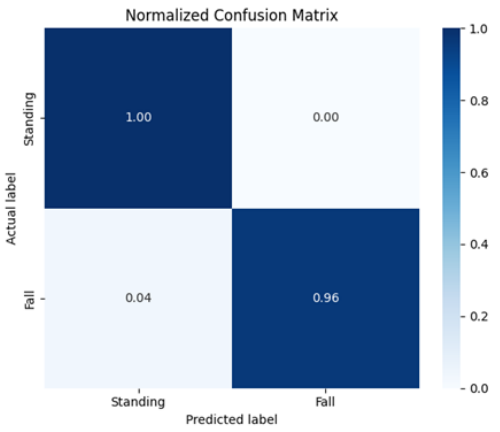

Figure 5. Multi-person scenarios fall detection confusion matrix

Table 5. Accuracy of 10 multi-person fall detection

Scenarios	Sensitivity	Precision	F1 score
1 subject	0.989	1.000	0.994
2 subjects	0.978	1.000	0.989
3 subjects	0.978	1.000	0.989
4 subjects	0.989	1.000	0.994
5 subjects	0.978	1.000	0.989
6 subjects	0.962	1.000	0.981
7 subjects	0.973	1.000	0.982
8 subjects	0.944	1.000	0.972
9 subjects	0.939	1.000	0.969
10 subjects	0.935	1.000	0.961

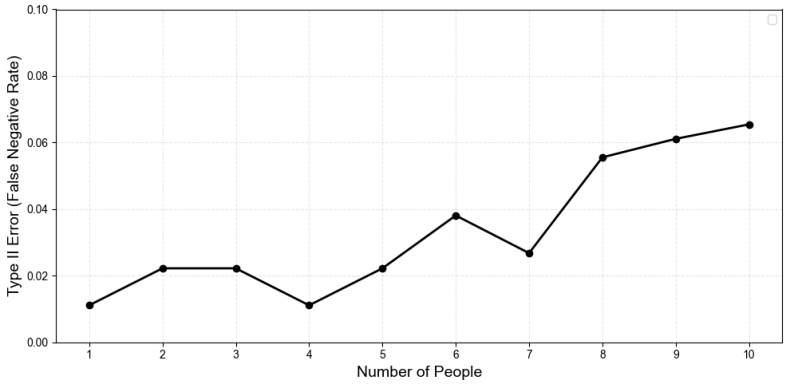

Figure 6. False negative rate of fall detection with different numbers of subjects

Accuracy of the radar system in fall-like Activities of Daily Living scenarios

The results of further investigation of fall-like Activities of Daily Living (ADLs) show a significant decrease in system accuracy of 76.8% for the threshold determined in our multi-person scenario trial, as shown in the Figure 7. The detection algorithm was then updated and refined by performing a grid search and LOOCV using ADLs trial data. The results of the updated thresholds (Figure 8) demonstrate an improvement in the accuracy of 86.5%, in which the parameters of vertical velocity and stillness height were added to the threshold parameters by performing Grid Search and LOOCV.

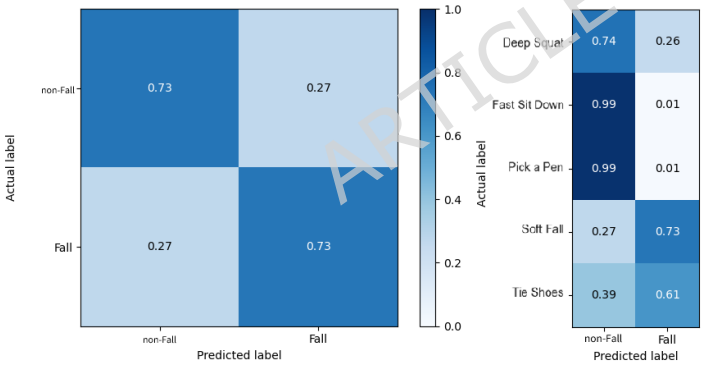

Figure 7. Fall-like ADLs scenarios confusion matrix with multi-person trial thresholds

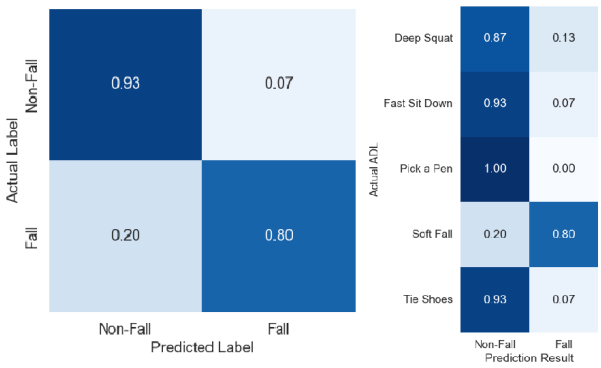

Figure 8. Fall-like ADLs scenarios confusion matrix with LOOCV adjusted thresholds

Fall occurrence time measurement

A time delay of 3.06 ± 2.08 seconds was persistently observed between the two signals across all experimental trials, according to the results of cross-correlation analysis. Moreover, our mmWave radar system presents similar accuracy for sensing simulated fall events compared to a few fall detection studies based on IMU measurements[4,25,26]. Indicating the development potential of mmWave technology in motion detection. Figure 9 demonstrates typical data of IMU G value and mmWave z-axis data in a trial.

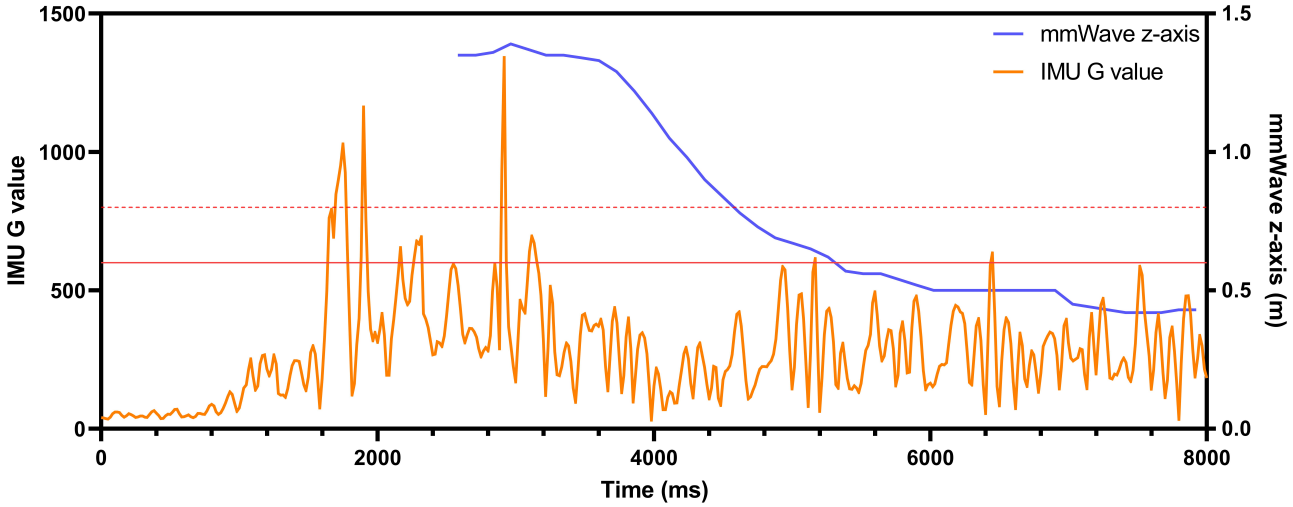

Figure 9. IMU G value vs. mmWave z-axis data

Discussion

This study investigated the fall detection capabilities of a mmWave radar system for multiple persons in large-scale indoor configurations. Unlike previous studies that focused on developing highly accurate radar systems for monitoring a single subject and a small detection zone[9,10,14,16–18], this study deployed multiple radar sensors to monitor a large indoor area. This study presented an overall fall detection accuracy of 97.9% in a large indoor detection area (area of 144 m^2, including a structural column) with a 4-radar sensor system. Past studies conducted their experiment in a small area of 3 m^2[16], 9 m^2[18], 12 m^2[9], 16.8 m^2[15], and 25 m^2[10], which limits the applicability of mmWave in a larger space. With an accuracy of 97.9%, our work provides evidence-based support for mmWave applications in a larger detection area. Meanwhile, the presence of a study design of structural column in the detection area was added in this study, which may be the reason why data in this work are less accurate compared those of (99.5%) Alhazmi et al[9], Yao et al[17], Kittiyanpunya et al[18] results and (98.9%) Liang et al[14] results (Table 6).

A 4-radar system was established in this study, compared to a 3-radar system in the study of Shen et al[15], detecting a 16.8 m^2 area; our system was deployed in a larger space of 144 m^2. Instead of covering the entire human body with a detection zone, Shen et al only detected the partial human body with every radar and further combined the point cloud in the data processing procedure, which could cause a lower detection accuracy of 96.%. In our work, the radars were placed to cover at least one third of the 144 m^2 area, with the system integrating the point cloud data of a whole human body. In addition, compared with Shen's study, we had added a maximum of 10 subjects to further evaluate the effect of the number on the mmWave detection accuracy. The type II error was 2.2%, 1.8%, and 2.1% in their study, which was not sufficient to analyze the trend. Our 10 scenarios' results present a strong correlation between the number of subjects and FNR ($r = 0.895$, $p < 0.001$), providing statistical evidence for the trend of elevated FNR in multi-person scenarios.

Single radar azimuth analysis demonstrates that the effective detection field of view (FOV) in our study is 90°, rather than the 120° as reported in the literature, but the effective detection range is similar, 3-6 meters[9,10]. This could be the consequence of expanding the detection area from 12 m^2[9] and 25 m^2[10] to 144 m^2, due to the limitation of mmWave technology. The results also indicate that the error distance is negatively correlated with the number of radar sensors, suggesting that detailed monitoring is possible using mmWave technology. As more radar sensors are deployed, the accuracy of object detection and tracking increases, reducing measurement errors and enhancing the overall monitoring performance. This finding highlights the effectiveness of the multi-radar approach in achieving more precise and comprehensive spatial analysis; in addition, it also makes up for the lack of data from multiple radars.

This study has several limitations. First, only 10 subjects were included in the experiment. A wider range of subjects with different characteristics will be necessary to further develop and validate the system. Second, the fall detection accuracy of 97.9% was limited in the simulated soft fall by 10 subjects, which couldn't fully represent the real scenario. A real fall could include the kinematics of 'reactive stepping failures' or 'vertical collapse' seen in frail elderly populations. However, inducing actual falls into trials in high-risk groups is ethically restricted. Third, the decreased accuracy of the mmWave system in ADLs indicates that a further comprehensive investigation of the robustness of the mmWave system in different ADLs is needed, and would also be conducted in our future studies to ensure the clinical applicability. Fourth, there would be a variety of obstacles in real-life scenarios, thus it may be necessary to further investigate the factors of the mmWave system. In

real-world scenarios, various types of obstacles may affect the performance of the mmWave system differently. Fifth, although the strategy of deploying multiple radar devices could improve the accuracy of the fall detection, the effect of the obstacle on the mmWave system wasn't analyzed in this study. During our trial, the mmWave detection of the human body could fail when the subjects were standing close to the central column, which could be the main reason for the loss of accuracy. Therefore, further investigation is needed to assess how different obstacles influence signal propagation, reflection, and attenuation. Future studies should explore these factors to enhance the system's adaptability and reliability in diverse environments. Finally, the detection latency of 3.49 ± 2.20 seconds in mmWave against IMU sensors couldn't fit the needs of injury prevention (<300ms required)[27]. However, for the post-fall rescue, a latency of around 3.5 seconds is clinically negligible for preventing the long lie fall, ensuring the system fits the golden window for acute nursing response [28,29].

The integration of mmWave sensors into healthcare practices not only enhances patient monitoring and safety but also supports proactive interventions, ultimately contributing to better health outcomes for vulnerable populations, particularly the elderly. In contrast to wearable sensors or cameras, mmWave radar technology preserves user privacy while continuously monitoring movement[15]. It detects falls by analyzing motion patterns, velocity, and real-time changes in body posture[9]. A significant advantage of mmWave radar in fall detection is its high accuracy, which is achieved through advanced signal processing and machine learning algorithms that effectively differentiate between falls and normal activities[30]. In this study, the mmWave system presents an overall predictability of (ROC = 0.979, $p < 0.001$) and an accuracy of 86.5% in ADLs trial, indicating the potential of mmWave technology. Furthermore, the ability of mmWave sensors to operate in various lighting conditions and their immunity to environmental factors such as dust or smoke enhance their reliability in diverse settings[31]. As the technology continues to evolve, we can expect further advancements in algorithms and data analytics that will improve the accuracy of fall risk assessments and mobility evaluations. The non-intrusive nature of mmWave sensors eliminates the need for wearable devices, enhancing comfort for long-term use. Additionally, the protection of privacy is a critical benefit; unlike cameras, mmWave radar does not capture identifiable images. Real-time alerts generated by this technology facilitate immediate intervention by caregivers, thereby reducing response times and enhancing overall safety. mmWave radar technology signifies substantial advancements in clinical fall detection applications. In hospital and long-term care environments, it facilitates continuous fall risk assessments, thereby enhancing patient safety and enabling proactive interventions. In the realm of home healthcare and telemedicine, mmWave radar supports real-time remote monitoring, allowing for the early identification of fall risks and timely clinical responses. Moreover, in rehabilitation and mobility assessment contexts, mmWave radar provides objective measurements of recovery following surgical procedures or strokes. This capability contributes to data-driven clinical decision-making, ultimately improving patient outcomes.

Looking ahead, the future of mmWave technology in fall detection and screening will prioritize enhancing accuracy through the development of advanced algorithms.[32–37] The integration of artificial intelligence (AI)[9] and the Internet of Things (IoT)[4] will facilitate real-time monitoring, while multi-sensor fusion techniques will enable more comprehensive detection capabilities. Key priorities will also include bolstering privacy and security measures, expanding remote monitoring capabilities for telehealth applications, and emphasizing strategies for early intervention and prevention. These advancements aim to improve healthcare outcomes, enhance patient safety, and revolutionize healthcare practices by leveraging mmWave technology for more effective fall detection and screening solutions. Both IMUs and mmWave technology serve as valuable tools for fall detection and gait analysis in clinical settings. While IMUs provide detailed, wearable data that can capture nuanced movements, mmWave technology offers a non-invasive alternative that respects patient privacy. Together, these technologies can significantly enhance patient monitoring, improve safety, and inform rehabilitation strategies, ultimately leading to better healthcare delivery and patient care.

Table 6. Overview of the mmWave studies with detection area and overall accuracy

Ref.	Fall detection data process method	Maximum number of detected people	Size of detection area	Overall Accuracy
[9]	3D Point cloud	1	12 m^2	99.5%
[10]	3D Point cloud	1	25 m^2	92.2%
[15]	3D Point cloud	3	16.8 m^2	96.3%
[14]	3D Point cloud	1	Not mentioned	98.9%
[16]	Range-Time, Doppler Time-Map	1	3 m^2	96.92%
[18]	1D point cloud, Doppler velocity	1	9 m^2	99.5%
[17]	Range-velocity, Range-angle Map	1	Not mentioned	99.5%
Our study	3D Point cloud	10	144 m^2	97.9%

Conclusion

This study evaluated the usability of a mmWave radar system for fall detection through large-scale, realistic indoor trials, validating its performance against video ground truth. The mmWave system demonstrates a high predictability of 97.9% accuracy of simulated fall events in a detection zone of 12 $\times$ 12 meters, despite a structural column present, demonstrating the capability of this technology. However, further ADL scenario trials have presented a lower accuracy of 86.5%. Cross-correlation analysis showed an average time delay of 3.06 ± 2.08 seconds between IMU measurement and mmWave system; The correlation of acceleration was found in further investigation ($rs = 0.944$, $p < 0.01$). Single radar presents the optimal detection ability in a FOV of 45° -45°, and the error distance was positively correlated with monitoring distance. Limitations regarding ecological validity remain, as simulated soft falls differ biomechanically from actual falls. Therefore, future research needs to conduct more advanced motion analysis on various fall scenarios. Furthermore, the system's performance is bounded by the standard GTRACK implementation and the specific 144 m² test layout, where obstacle-induced occlusion was not explicitly modeled. Current findings thus represent a multi-radar fusion baseline. Future work must therefore focus on advanced data association, systematic signal analysis for obstacle scenarios, and multi-site validation to enhance robustness across diverse real-world applications. This study supports that mmWave technology offers capabilities for fall accident monitoring in large indoor spaces with non-contact detection, privacy protection, convenience, and remote monitoring.

Data Availability

Most of the data generated during this study are included in this published article and its supplementary information files. However, the video data during the current study are not publicly available due to privacy concerns of the participants, but are available from the corresponding author on reasonable request.

Funding Declaration

Funding: National Science and Technology Council of Taiwan (NSTC 112-2221-E-182-008-MY2 and NSTC 114-2221-E-182-031-MY3).

Acknowledgment

We thank Jorjin Technology Co., Ltd. (New Taipei City, Taiwan) for technical support.

References

1. Murphy, S. L., Kochanek, K. D., Xu, J. *et al.* Deaths: Final data for 2021, DOI: 10.15620/cdc/158787 (2024). Available from: https://www.ncbi.nlm.nih.gov/books/NBK613913/.
2. Research, G. V. patient safety and risk management software market size, share trends analysis report by type, by deployment type (cloud, on-premise), by end-use (hospitals, ambulatory care centers, long-term care centers), by region, and segment forecasts, 2024 - 2030 (2023).
3. Feng, G., Mai, J., Ban, Z., Guo, X. & Wang, G. Floor pressure imaging for fall detection with fiber-optic sensors. *IEEE Pervasive Comput.* **15**, 40–47, DOI: 10.1109/MPRV.2016.27 (2016).
4. Lin, H. C., Chen, M. J., Lee, C. H., Kung, L. C. & Huang, J. T. Fall recognition based on an imu wearable device and fall verification through a smart speaker and the iot. *Sensors (Basel)* **23**, DOI: 10.3390/s23125472 (2023).
5. Lin, H.-C., Chen, M.-J., Lee, C.-H., Kung, L.-C. & Huang, J.-T. Fall recognition based on an imu wearable device and fall verification through a smart speaker and the iot. *Sensors* **23**, 5472 (2023).
6. Capra, M. *et al.* Assessing the feasibility of augmenting fall detection systems by relying on uwb-based position tracking and a home robot. *Sensors (Basel)* **20**, DOI: 10.3390/s20185361 (2020).
7. Mehrotra, P., Chatterjee, B. & Sen, S. Em-wave biosensors: A review of rf, microwave, mm-wave and optical sensing. *Sensors (Basel)* **19**, DOI: 10.3390/s19051013 (2019).
8. Wang, H. *et al.* Millimeter waves in medical applications: status and prospects. *Intell. Medicine* **4**, 16–21, DOI: 10.1016/j.imed.2023.07.002 (2024).
9. Alhazmi, A. K. *et al.* Intelligent millimeter-wave system for human activity monitoring for telemedicine. *Sensors (Basel)* **24**, DOI: 10.3390/s24010268 (2024).
10. Rezaei, A. *et al.* Unobtrusive human fall detection system using mmwave radar and data driven methods. *IEEE Sensors J.* **23**, 7968–7976, DOI: 10.1109/JSEN.2023.3245063 (2023).

11. Chen, F.-K. *et al.* Feasibility study for apnea screening in patients' homes using radar and machine learning method, DOI: 10.1109/bibe55377.2022.00065 (2022).

12. Xiang, Y., Guo, J., Chen, M., Wang, Z. & Han, C. Mae-based self-supervised pretraining algorithm for heart rate estimation of radar signals. *Sensors (Basel)* **23**, DOI: 10.3390/s23187869 (2023).

13. Cao, Z., Mei, G., Guo, X. & Wang, G. Virteach: mmwave radar point-cloud-based pose estimation with virtual data as a teacher. *IEEE Internet Things J.* **11**, 17615–17628, DOI: 10.1109/jiot.2024.3359209 (2024).

14. Liang, T. *et al.* Fall detection system based on point cloud enhancement model for 24 ghz fmcw radar. *Sensors (Basel)* **24**, DOI: 10.3390/s24020648 (2024).

15. Shen, Z., Nunez-Yanez, J. & Dahnoun, N. Advanced millimeter-wave radar system for real-time multiple-human tracking and fall detection. *Sensors (Basel)* **24**, DOI: 10.3390/s24113660 (2024).

16. Wang, B., Zhang, H. & Guo, Y.-X. Radar-based soft fall detection using pattern contour vector. *IEEE Internet Things J.* **10**, 2519–2527, DOI: 10.1109/jiot.2022.3213693 (2023).

17. Yao, Y. *et al.* Fall detection system using millimeter-wave radar based on neural network and information fusion. *IEEE Internet Things J.* **9**, 21038–21050, DOI: 10.1109/jiot.2022.3175894 (2022).

18. Kittiyanpunya, C., Chomdee, P., Boonpoonga, A. & Torrungrueng, D. Millimeter-wave radar-based elderly fall detection fed by one-dimensional point cloud and doppler. *IEEE Access* **11**, 76269–76283, DOI: 10.1109/ACCESS.2023.3297512 (2023).

19. Shi, J., Zhang, Q., Shi, Q., Chu, L. & Braun, R. Pedestrian pose recognition based on frequency-modulated continuous-wave radar with meta-learning. *Sensors (Basel)* **24**, DOI: 10.3390/s24092932 (2024).

20. Wang, Q. *et al.* Frequency-modulated continuous wave radar respiratory pattern detection technology based on multifeature. *J Heal. Eng* **2021**, 9376662, DOI: 10.1155/2021/9376662 (2021).

21. Peake, G. Building a multipatient contactless vital signs sensor for at-home use with mmwave radar sensors. In *Analog Design Journal*, 1–6 (2023).

22. Hanifi, K. & Karsligil, M. E. Elderly fall detection with vital signs monitoring using cw doppler radar. *IEEE Sensors J.* **21**, 16969–16978, DOI: 10.1109/JSEN.2021.3079835 (2021).

23. Lu, J. & Ye, W.-B. Design of a multi-stage radar-based human fall detection system. *IEEE Sensors J.* **22**, 1–1, DOI: 10.1109/JSEN.2022.3177173 (2022).

24. Chen, Y., Yuan, J. & Tang, J. A high precision vital signs detection method based on millimeter wave radar. *Sci Rep* **14**, 25535, DOI: 10.1038/s41598-024-77683-1 (2024).

25. Tseng, C. K., Huang, S. J. & Kau, L. J. Wearable fall detection system with real-time localization and notification capabilities. *Sensors (Basel)* **25**, DOI: 10.3390/s25123632 (2025). 1424-8220 Tseng, Chin-Kun Huang, Shi-Jia Kau, Lih-Jen Orcid: 0000-0001-8115-3751 NSTC 113-2221-E-027-082/National Science and Technology Council, Taiwan/ Journal Article Switzerland 2025/06/27 Sensors (Basel). 2025 Jun 10;25(12):3632. doi: 10.3390/s25123632.

26. Tang, J. *et al.* Synthetic imu datasets and protocols can simplify fall detection experiments and optimize sensor configuration. *IEEE Transactions on Neural Syst. Rehabil. Eng.* **32**, 1233–1245, DOI: 10.1109/TNSRE.2024.3370396 (2024).

27. Jung, H. *et al.* Enhanced algorithm for the detection of preimpact fall for wearable airbags. *Sensors* **20**, 1277, DOI: 10.3390/s20051277 (2020).

28. Kubitza, J., Haas, M., Keppeler, L. & Reuschenbach, B. Therapy options for those affected by a long lie after a fall: a scoping review. *BMC Geriatr.* **22**, 582, DOI: 10.1186/s12877-022-03258-2 (2022).

29. Fleming, J. & Brayne, C. Inability to get up after falling, subsequent time on floor, and summoning help: prospective cohort study in people over 90. *BMJ* **337**, a2227, DOI: 10.1136/bmj.a2227 (2008). Article No. a2227.

30. Alanazi, M. A. *et al.* Towards a low-cost solution for gait analysis using millimeter wave sensor and machine learning. *Sensors (Basel)* **22**, DOI: 10.3390/s22155470 (2022).

31. Dang, X. *et al.* Pggait: Gait recognition based on millimeter-wave radar spatio-temporal sensing of multidimensional point clouds. *Sensors (Basel)* **24**, DOI: 10.3390/s24010142 (2023).

32. Zhao, C. *et al.* mm-Fall: Practical and Robust Fall Detection via mmWave Signals . *IEEE Transactions on Mob. Comput.* **24**, 8747–8760, DOI: 10.1109/TMC.2025.3557504 (2025).

33. Yao, Y. *et al.* Unsupervised-learning-based unobtrusive fall detection using fmcw radar. *IEEE Internet Things J.* **11**, 5078–5089, DOI: 10.1109/JIOT.2023.3301887 (2024).

34. Li, W. *et al.* Scl-fall: Reliable fall detection using mmwave radar with supervised contrastive learning. *IEEE J. Sel. Areas Sensors* **1**, 237–248, DOI: 10.1109/JSAS.2024.3481205 (2024).

35. Yao, Y. *et al.* Fall detection system using millimeter-wave radar based on neural network and information fusion. *IEEE Internet Things J.* **9**, 21038–21050, DOI: 10.1109/JIOT.2022.3175894 (2022).

36. Yu, Y. S., Wie, S., Lee, H., Lee, J. & Kim, N. H. Long short-term memory-based fall detection by frequency-modulated continuous wave millimeter-wave radar sensor for seniors living alone. *Appl. Sci.* **15**, DOI: 10.3390/app15158381 (2025).

37. Wu, T.-W., Fang, S.-H., Wu, H.-C., Liu, G. & Yan, K. Robust skeletal-graph reconstruction using mmwave radar and its application for human-activity recognition. *IEEE J. Sel. Areas Sensors* **2**, 199–211, DOI: 10.1109/JSAS.2025.3581498 (2025).